



## Aerosol route in processing of nanostructured phosphor materials<sup>#</sup>

Katarina Marinković<sup>1</sup>, Luz S. Gomez<sup>2</sup>, Maria E. Rabanal<sup>2</sup>, Lidija Mančić<sup>1</sup>, Olivera Milošević<sup>1,\*</sup>

<sup>1</sup>Institute of Technical Sciences of Serbian Academy of Sciences and Arts, K. Mihailova 35/IV, 11000 Belgrade, Serbia

<sup>2</sup>Universidad Carlos III de Madrid, Avda. de la Universidad 30, Leganes, Madrid, Spain

Received 23 February 2010; received in revised form 17 May 2010; accepted 23 August 2010

### Abstract

Among the methods currently used for nanophase processing, synthesis through dispersion phase (aerosol) enables generation of ultrafine powders with controlled stoichiometry. It represents a “bottom-up” chemical approach that provides control over a variety of important parameters enabling the formation of either amorphous, nanocrystalline or metastable phases. Particularly, the opportunities of the hot wall aerosol synthesis, i.e. spray pyrolysis, for the generation of ultrafine phosphor particles with uniformly distributed components, nano-clustered inner structure and luminescence properties is demonstrated in following systems:  $Gd_2O_3:Eu$ ,  $Y_2O_3:Eu$ ,  $(Y_{1-x}Gd_x):Eu$  and  $Y_3Al_5O_{12}:Ce$ , highlighting the research activities in the Institute of Technical Sciences of SASA, Serbia and the University Carlos III, Madrid, Spain in the framework of COST 539 Action.

**Keywords:** aerosol, nanoparticles, synthesis, phosphors, luminescence

### I. Introduction

The field of nanoscience and nanotechnology has an exciting progress in recent years, particularly regarding the control synthesis of ultrafine particles or nanoparticles that might have a great potential for use in solid-state functional materials and devices, like phosphors, sensors, catalysts, drug delivery carriers etc. [1] The key points important for the future research of nano-phased materials represent the ability for further improvement of material properties through nanostructuring and fundamental research of structure-properties relationship. The chemical synthesis routes, like liquid precipitation, sol-gel, hydrothermal methods or synthesis through aerosol, offer many advantages over conventional procedures for nanoscaled materials processing. Since the precursors are mixed at the molecular level in a solution, a high degree of structural homogeneity is achievable; doping is effective; surface area of powder produced is very high, leading to lower processing temperature. Compared to other processing

techniques, powder synthesis through aerosol routes represents a simple method for production of oxide, non-oxide, metal and composite powders of complex composition, either in amorphous, crystalline or nanocrystalline state [2]. Solution chemistry approaches offer design of materials at the molecular level, spherical particle morphology with full or hollow spheres, having narrow particle size distribution and a very homogeneous composition. Depending on how the thermal energy is provided to the precursors, affecting the most important particle formation parameters: residence time and temperature distribution, one can distinguish: hot-wall processing - spray pyrolysis, flame synthesis, self sustaining flame reactors and self combustion aerosol synthesis [3]. Hot-wall aerosol synthesis is based on the formation of aerosols of precursor solutions and control over the aerosol decomposition in a high temperature tubular flow reactor through the successive processes of droplet evaporation, drying, solute precipitation and decomposition. Since the heterogeneous gas/liquid-solid reaction occurs in a dispersed system-aerosol at the level of few micrometers sized droplets, compositional segregation is prevented and high heating rates (20–300°C/s) could be achieved [2]. During decomposition, the aerosol droplets undergo evaporation/drying, precipitation and thermolysis in a single-step process.

<sup>#</sup> These results were partially published in a review article “Aerosol route in processing of nanostructured functional materials”, KONA 27 (2009) 84–106

\* Corresponding author: tel: +381 11 2636994

fax: +381 11 2185263, e-mail: [olivera.milosevic@itn.sanu.ac.rs](mailto:olivera.milosevic@itn.sanu.ac.rs)

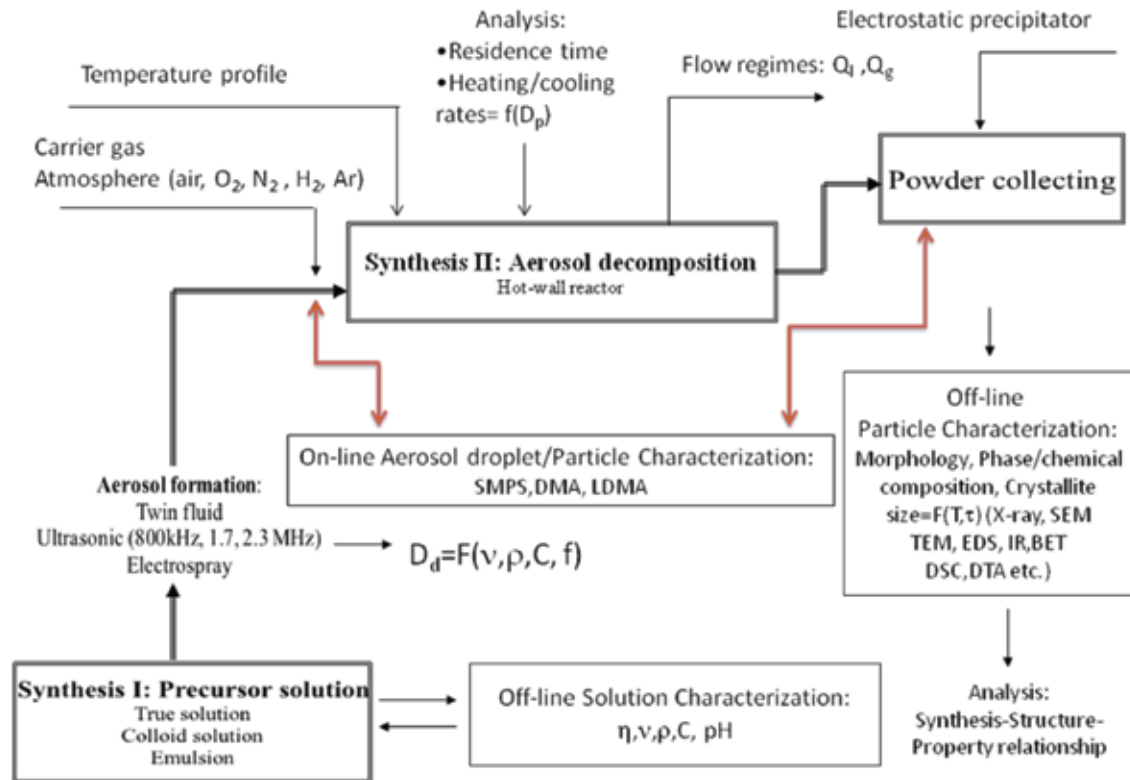


Figure 1. Schematic of the hot wall aerosol synthesis route, i.e. spray pyrolysis methodology [5]

Consequently, spherical, solid, agglomerate-free, either submicronic, nanostructured or nanoscaled particles are obtained through the mechanisms of primary nanoparticles coalescence, collision and sintering. Schematic of the hot-wall aerosol synthesis routes is presented in Fig. 1. *Synthesis I* refers to the chemical synthesis and solution preparation that could be in the form of true solutions, colloids or emulsions. The modification of the chemistry of the solution, i.e. additives like glycine, urea, sucrose etc. alters the morphology of the particles derived as well as the particle size, size distribution and agglomeration state. The precursors and precursor's chemistry are usually characterized for their physico-chemical properties since there is a strong relationship between them and the droplet/particle size [4]. Liquid atomization and aerosol formation occur for the certain values of the acoustic waves amplitude formed by ultrasonic beam (100 KHz–10 MHz). Depending on the atomization technique, either monodispersed or polydispersed droplets could be generated. More about the manner of aerosol formation and equations that govern droplets and particle size distribution was published previously [5]. The generated aerosol is carried out by the flowing gas stream into high-temperature tubular flow reactor. During the main process, denoted as *Synthesis II*, aerosol droplets undergo evaporation, drying and solute precipitation in a single-step process caused by the mechanisms of heat and mass transfer inside the droplets and between the droplets and surrounding gas. Such mechanism enables high surface reaction, solution

stoichiometric retention as well as segregation suppression to the droplet scale.

The primary particles arise through the thermally induced processes of nuclei formation, collision and coalescence, resulting in final spherical arrangement called “secondary particles”. The secondary particle size and size distribution are mainly influenced by the properties of aerosol generator and precursor solutions. Primary particles, that represent either crystallites or block-mosaic assemblies could coalesced entirely or densified with existing nanoporosity influencing the morphology and size of secondary particles. Processing of nanoparticles can be achieved directly from nano-sized droplets, from very dilute solutions or from submicronic secondary particles, that offer a composite nanograin particle structure [6,7]. Salt assisted spray pyrolysis (SAD) enable releasing the nano-scaled primary particles by modification the solution chemistry and preventing formation of aggregated primary particles into the secondary particles [8].

The potentials of the aerosol routes for making solid-states structures at the nano-size level are virtually unlimited, providing possibilities for their unique applications in electronics, optoelectronics, catalysis, energy conversion systems, drug delivery etc. In the framework of our recent research, the synthesis of fine particles have been established for following materials: ZnO [9], ZnO-Pt(IV) [10], ZnO- Ru(III) [11] and ZnO-Cr<sub>2</sub>O<sub>3</sub> spinel phase [7]. Achievements attained in the synthesis of phosphor materials [5,12–25], will be reviewed here.

## II. Phosphors

Phosphors represent inorganic crystal structures capable of emitting definite quantities of radiation within visible and/or ultraviolet spectrum as a result of excitation by an external energy source such as electron or a photon beam [26,27]. Such properties of these materials are an outcome from the atomic state interactions that occur between luminescent centres and the host lattice material after the excitation. Rare earth ions ( $\text{Eu}^{2+}$ ,  $\text{Eu}^{3+}$ ,  $\text{Ce}^{3+}$ ,  $\text{Tm}^{3+}$ ,  $\text{Tb}^{3+}$ ,  $\text{Nd}^{3+}$ ) and transition metal ions ( $\text{Cr}^{3+}$ ,  $\text{Mn}^{2+}$ ) are commonly used as luminescent centres [28]. The important properties that luminescent materials should have are brightness, spectral energy distribution and decay time [29].

### $\text{Gd}_2\text{O}_3:\text{Eu}^{3+}$

Gadolinia doped with europium has been used in several applications for display devices as effective red phosphor material having improved stability in high vacuum and the absence of corrosive gas emissions under electron bombardment [30]. As part of a program to develop high grade phosphor particles, spherical in shape, agglomerated-free and with a narrow size distribution, nanostructured, spherical  $\text{Gd}_2\text{O}_3:\text{Eu}^{3+}$  phosphor particles sizing below 800 nm were synthesized from ultrasonically generated common nitrates solutions, Fig. 2.

The particle inner structure (Fig. 2b) implies that nano-sized primary particles are assembled in a spherical secondary particle, Fig. 2a. Visual inspection of the particle morphology is done by means of STEM nanotomography corresponding to the particle annealed at low temperature ( $900^\circ\text{C}/12\text{h}$ ). The contrast obtained with HAADF-STEM implies bright and dark areas in a spherical shaped particle sized approx. 500 nm, indicating the presence of voids and a rough particle surfaces (Fig. 2c). In the reconstructed image (Fig. 2d), the better contrast than the original image confirms the porous surfaces. Particle roughness and agglomeration state are very important factors that affect the luminescence signal. Beside it, the sensitization of the as-prepared particles is a critical stage in phosphor preparation and sensitivity improves with increasing the crystallinity and homogenization of the Eu dopants within the particles. Success in this processing have been obtained with additional thermal treatments of the as-prepared particles above  $800^\circ\text{C}$ , where the thermally induced interparticle sintering did not occur and initially obtained morphological features were preserved [12,24]. Uniform compositional distribution of constitutive elements is confirmed by EFTEM-EELS spectrum presented in Fig. 3. The comparison between the spectrum indicates the in-

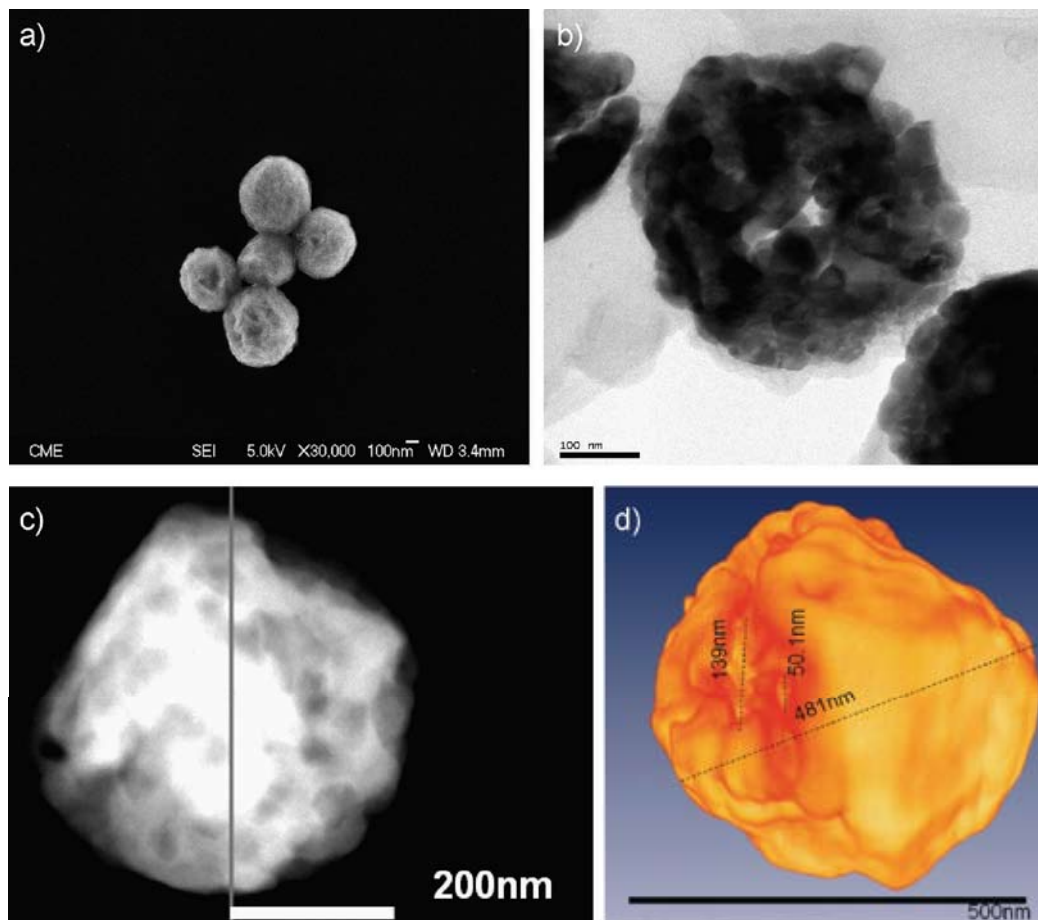
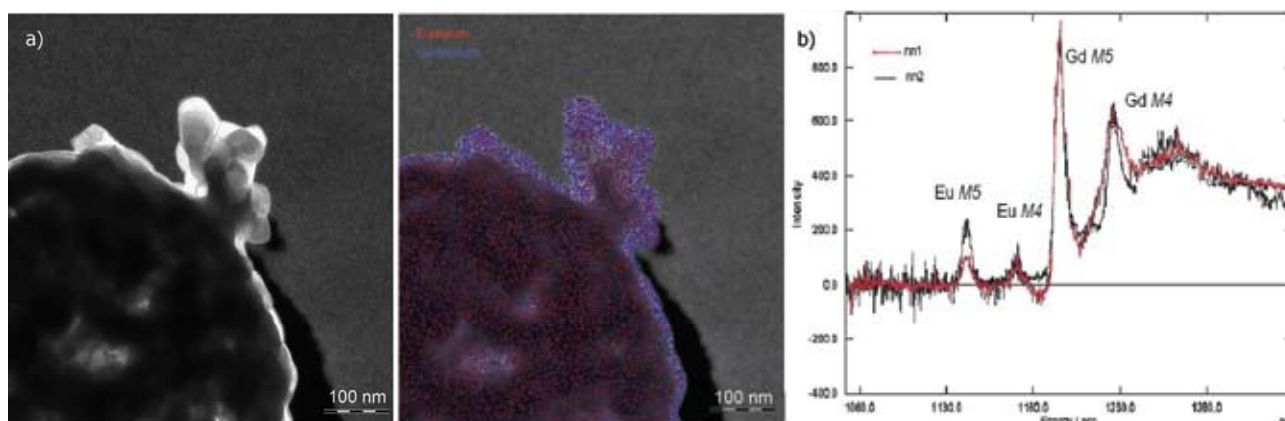


Figure 2.  $\text{Gd}_2\text{O}_3$  particles: surface morphology by FE-SEM (a), inner particle structure by TEM (b) STEM image of the tomography tilt series (c) and reconstructed tomography image (d)



**Figure 3.** EFTEM image (a) and EFTEM-EELS spectra for  $\text{Gd}_2\text{O}_3:\text{Eu}^{3+}$  particles additionally annealed at  $900^\circ\text{C}/12\text{h}$  (grey line) and  $100^\circ\text{C}/12\text{h}$  (black line); ELNES region show the Gd M4 and Gd M5 signal ( $\sim 1185$  eV– $1187$  eV) and the Eu M5 and Eu M4 signal ( $\sim 1131$  eV– $1186$  eV)

corporation of the Eu in the Gd matrix, while no changes in the energy and intensity  $M4/M5$  ratio (0.83) indicates a +3 oxidation state in the samples with different Eu content (Fig. 3b).

Host gadolinium oxide exhibits two polymorphic forms, low temperature (cubic) and high temperature (monoclinic), so several studies dealing with the investigation of  $\text{Gd}_2\text{O}_3$  crystal phases development during aerosol synthesis and their relationship with luminescence properties were reported [31,32]. XRPD revealed here the presence of two cubic phases in as-prepared powders: a *bcc* phase with *Ia3* space group ( $a \approx 10.829(3)$  Å); and a *fcc* phase with *Fm-3m* space group ( $a \approx 5.6242(1)$  Å) for the  $\text{Eu}^{3+}$  less doping concentration [33]. In addition, HRTEM analysis (Fig. 4) indicates the locally appearance of a monoclinic phase with *c2/m* symmetry in this sample, too.

The local appearance of the higher density metastable monoclinic structure is probably a consequence of the extreme synthesis conditions during spray pyrolysis, i.e. high heating rates and short residence time and attributable to the Gibbs-Thomson effect, associated with increased surface tension with nanostructuring [12]. After thermal treatment only the cubic *Ia3* phase has been

observed, with the cell parameters affected with  $\text{Eu}^{3+}$  doping concentration, followed with progressive increase in crystallite size.

Luminescence studies carried out in  $\text{Gd}_2\text{O}_3:\text{Eu}^{3+}$  phosphor system have demonstrated that annealing and crystalline phases control both the thermoluminescence and radioluminescence signals [12]. Characteristic bands in the emission spectra are assigned to  $\text{Eu}^{3+}$  ion radiative  ${}^5\text{D}_0 \rightarrow {}^7\text{F}_i$  ( $i = 0, 1, 2, 3, 4$ ) transitions. In all the samples maximum intensity peak is at 611 nm wavelength belonging to  ${}^5\text{D}_0 \rightarrow {}^7\text{F}_2$  transition [33,34]. All observed transitions are due to the  $\text{Eu}^{3+}$  in  $\text{C}_2$  crystallographic site except one line, at 581 nm (attributed to  ${}^5\text{D}_0 \rightarrow {}^7\text{F}_1$  transition) that belongs to  $\text{Eu}^{3+}$  in  $\text{S}_6$  crystallographic site.

#### $\text{Y}_2\text{O}_3:\text{Eu}^{3+}$

Yttria represents one of the best host materials for rare earth ions due to the fact that its ionic radii and crystal structure are very similar to the ones of the rare earth ions.  $\text{Y}_2\text{O}_3$  doped with europium is a well known red phosphor material employed in modern high-resolution display devices such as plasma display panels (PDP) and field emission displays (FED) [35]. Here, the nanostructured particles of  $\text{Y}_2\text{O}_3$  doped with  $\text{Eu}^{3+}$

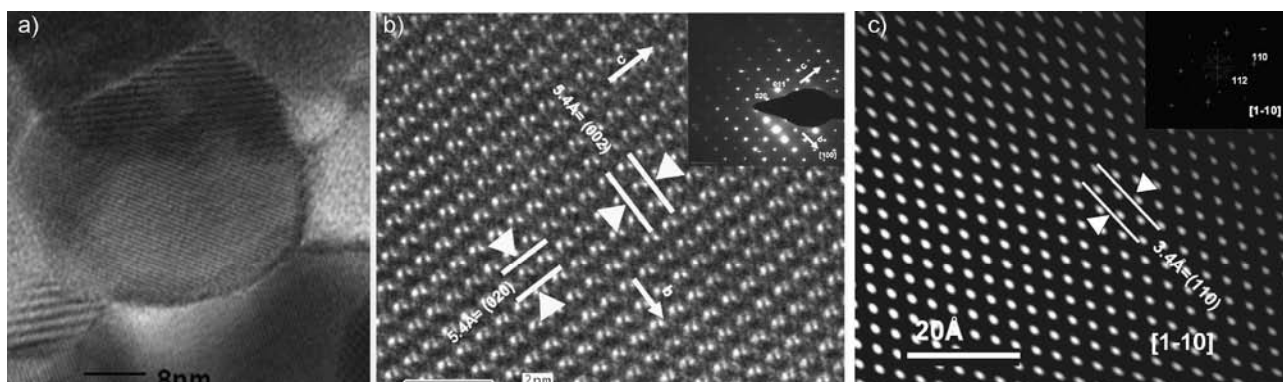


**Figure 4.** HRTEM of  $\text{Gd}_2\text{O}_3:\text{Eu}^{3+}$  particles: primary nano-particles associated with a defect structure (a); cubic phase with *Ia3* symmetry taken along the [100] zone with (002) and (020) atomic planes resolved (b); monoclinic phase with *c2/m* symmetry taken along the [1-10] zone axis with (110) atomic distance resolved (c)

were processed through the spray pyrolysis method from nitrate precursors [23]. Synthesis was carried out with an ultrasonic aerosol device operating at 1.3 MHz in air atmosphere connected with a triple-zone tubular flow reactor (200–700–900°C). Particles were submitted to post-thermal treatments at temperatures of 1000 to 1200°C for 12 h in order to increase the crystallinity and uniform distribution of doped centres. The particles obtained were spherical, having narrow size distributions, high compositional homogeneity and unagglomerated (Fig. 5). Exceptionally, inter particle sintering and neck formation were noticed in the case of the samples thermally treated at 1200°C [16,34]. The  $Y_2O_3$  cubic  $Ia3$  phase has been identified by XRD and TEM-HRTEM/FFT in both as-prepared and thermally treated samples. Rietveld refinement revealed that crystallite size of the as-prepared powders was around 20 nm while sufficient energy supply during the thermal treatment led to crystallite growth (40–130 nm for annealing temperatures 1000–1200°C, respectively) and affected structural relaxation (lower values of microstrain in comparison to the values for as-prepared samples), Table 1.

Determination of photoluminescent characteristics showed typical emission spectra of  $Eu^{3+}$  ion incorporated into yttrium oxide. Emission spectra were obtained at room temperature through excitation of  $Eu^{3+}$  ion into  ${}^5L_6$  energy level under 393 nm wavelength (Fig. 6). The emission lines of  $Eu^{3+}$  were ascribed to  ${}^5D_0 \rightarrow {}^7F_j$  ( $j = 1, 2, 3, 4$ ) spin forbidden  $f-f$  transitions and the main emission peak corresponded to clear red emission at 611 nm. Emission spectra consist out of sharp peaks, originating from  $Eu^{3+}$  ion incorporated into  $C_2$  sight, while only one weak line belonging to  $Eu^{3+}$  ion incorporated into  $S_6$  sight was observed. Maximum Stark splitting ( $\Delta E$ ) of the  ${}^7F_1$  manifold, occurring under the influence of the crystal field, was in agreement with theoretical values  $Y_2O_3:Eu^{3+}$  ( $\Delta E(Y_2O_3) = 355 \text{ cm}^{-1}$ ) [36]. Based on the fluorescence decay curves of the  ${}^5D_0$  emitting level it was concluded that applied synthesis method leads to the formation of nanostructured powders having longer lifetimes in comparison to  $Y_2O_3:Eu^{3+}$  in its bulk form [37]. Also, it was shown that samples with higher doping concentration had lower  ${}^5D_0$  lifetimes implying that at higher doping level concentration quenching occurs (Table 1).

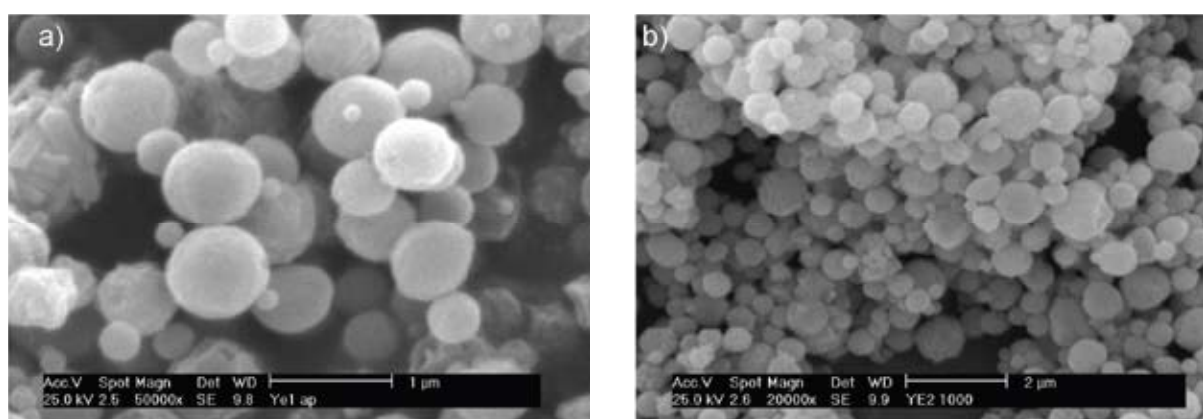


Figure 5. SEM of  $(Y_{0.95}Eu_{0.05})_2O_3$  obtained at 900°C (a) and  $(Y_{0.90}Eu_{0.1})_2O_3$  thermally treated at 1000°C (b)

Table 1. Main structural parameters derived through Rietveld refinement and characteristics of the luminescent measurements for  $Y_2O_3:Eu^{3+}$  system [23]

	$(Y_{0.95}Eu_{0.05})_2O_3$				$(Y_{0.9}Eu_{0.1})_2O_3$			
	AP	1000°C	1100°C	1200°C	AP	1000°C	1100°C	1200°C
$cs$ [nm]	19.14	40.55	60.06	129.53	20.11	40.94	66.99	132.89
$a$ [Å]	10.620	10.616	10.616	10.616	10.632	10.628	10.623	10.628
$ms$ [%]	0.432	0.189	0.0607	0.0963	0.529	0.197	0.0794	0.0402
${}^5D_0 \rightarrow {}^7F_0$ ( $C_2$ ) [nm]	580.3	580.4	580.4	580.4	580.4	580.4	580.4	580.4
${}^5D_0 \rightarrow {}^7F_1$ ( $S_6$ ) [nm]	582.1	582.3	582.2	582.2	582.2	582.0	582.1	582.1
	587.1	587.2	587.1	587.2	587.1	587.2	587.2	587.2
${}^5D_0 \rightarrow {}^7F_1$ ( $C_2$ ) [nm]	592.9	592.8	592.8	592.9	592.8	592.8	592.8	592.8
	599.2	599.1	599.2	599.4	599.2	599.2	599.2	599.2
$\Delta E$ [ $\text{cm}^{-1}$ ]	344.0	338.2	344.0	346.5	344	341	341	341
$\tau({}^5D_0 \rightarrow {}^7F_2)$ [ms]	1.47	1.46	1.40	1.42	1.24	1.21	1.14	1.14
$\tau_{avr}({}^5D_1 \rightarrow {}^7F_2)$ [ $\mu\text{s}$ ]	11.33	18.97	19.74	19.78	/	/	/	/

AP - as-prepared sample

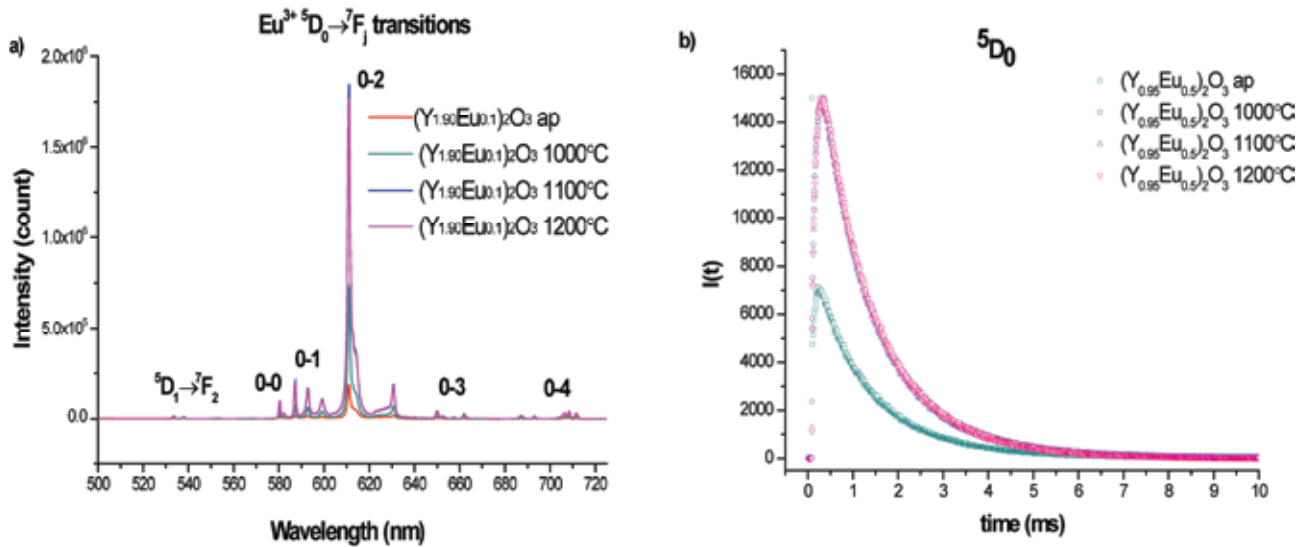


Figure 6. Emission spectra of  $(Y_{0.95}Eu_{0.05})_2O_3$  system (a) and lifetime values of  $(Y_{0.95}Eu_{0.05})_2O_3$  system under  $\lambda_{ex} = 393$  nm ( $\lambda_{em} = 611$  nm) (b) [23]

Analysis of lifetime values for  $Eu^{3+}5D_1$  emitting level for  $Y_2O_3$  with 5 at% of  $Eu^{3+}$  highlights the influence of thermally treatment. It was shown that as-prepared powders had a lower value of these parameter (around 11  $\mu s$ ) while the value for thermally treated was slightly higher (around 20  $\mu s$ ). Knowing that decrease of emission intensity from  $5D_1$  emitting level is due to increased probability of cross-relaxation mechanism which occurs [38], it was concluded that cross-relaxation effect was stronger in the case of as prepared samples. Above stated observations indirectly depicted more homogeneous distribution of  $Eu^{3+}$  ions in case of the annealed samples.

$(Y,Gd)_2O_3:Eu^{3+}$

The incorporation of gadolinium in the yttria matrix may significantly contribute to the luminescent properties and X-ray absorption coefficient, thus, increasing the field of application in optoelectronic devices such as ceramic scintillators for computed tomography.  $(Y_{1-x}Gd_x)_2O_3:Eu^{3+}$  system, where the gadolinium content was varied ( $x = 0.25, 0.50, 0.75$ ), has been synthesized throughout the same conditions as  $Y_2O_3:Eu^{3+}$ . TEM investigations revealed that these systems exhibit the same morphological features as yttrium oxide system. Additionally SAED patterns revealed polycrystalline nature of the particles, while the ring width implied high defect content in as-prepared powders, Fig. 7a. As-prepared samples with composition  $x = 0.25, 0.50$  had solely  $Ia3$  phase, but the sample compositionally closest to pure  $Gd_2O_3$ , with  $x = 0.75$ , showed the same characteristics as gadolinium oxide synthesized under similar conditions, Fig. 7b. Apart from primary, cubic  $bcc$   $Ia3$  phase a second cubic  $fcc$  phase with  $Fm-3m$  space group was confirmed in as prepared samples [16,23]. In all thermally treated samples (1100°C, 12 h),  $Ia3$  phase is solely detected.

Observing the optical properties, the same characteristic emission spectra of  $Eu^{3+}$  ion were seen as in the case of pure  $Y_2O_3:Eu^{3+}$  system. Detailed analysis of the emission spectra showed that in the case of  $(Y_{1-x}Gd_x)_2O_3:Eu^{3+}$  system a linear increase of maximum Stark splitting ( $\Delta E$ ) occurs with the increase of gadolinium content/lattice parameters, Table 2. Since maximum splitting of the  $7F_1$  manifold is affected by crystal field strength parameter in a proportional way [23,29], the increase of  $\Delta E$  value with the increase of gadolinium content could be treated as a clear indication of almost perfect mixing in solid solutions.

When doped with 5 at% mixed  $(Y_{1-x}Gd_x)_2O_3:Eu^{3+}$  oxides, thermally treated at 1100°C, had similar lifetime values of  $5D_0$  emitting level in comparison to yttria with same doping concentration (around 1.4  $\mu s$ ). In the case of  $x = 0.50$ , doping was done with 5 and with 10 at% of  $Eu^{3+}$  and in these case  $5D_0$  lifetime of the sample with higher doping concentration was significantly smaller i.e. 0.86  $\mu s$ . It indicated concentration quenching and that  $(Y_{1-x}Gd_x)_2O_3:Eu^{3+}$  with  $x = 0.50$  and 10 at% of  $Eu^{3+}$  had inferior properties than the material in bulk form. Relatively high values of  $5D_1$  lifetimes for thermally treated  $(Y_{1-x}Gd_x)_2O_3:Eu^{3+}$  powders with 5 at% revealed, as in the case of  $Y_2O_3:Eu^{3+}$ , homogeneous distribution of the doping ion.

$Y_3Al_5O_{12}$  (YAG):  $Ce^{3+}$

The  $Y_3Al_5O_{12}$  (YAG) is optically isotropic material with high thermal conductivity. Doped with rare earth ions it represents very useful phosphor material for variety of display applications including cathode ray tube, low voltage field emission display, and backlight source. Specially cerium doped YAG ( $YAG:Ce^{3+}$ ), as a yellow-emitting component for the production of a white light, is a comprehensively studied previous years due to urgent demand for alternative light source in an illumi-

nation and display area. The broad  $\text{Ce}^{3+}$  emission band originates from the 4f-5d electronic transition with intensive side bands due to vibronic coupling to the lattice and local vibration modes in the YAG lattice. Due to this YAG: $\text{Ce}^{3+}$  easily convert blue emission from blue light emitting diode (LED) into white LED. Even a lack of cerium emission toward the red region can be suppressed by a co-doping ( $\text{Tb}^{3+}$ ) or cation substituting ( $\text{Ga}^{3+}$  or  $\text{Gd}^{3+}$ ) making presently this material to be the phosphor of choice in commercial white LEDs [40].

Processing of YAG: $\text{Ce}^{3+}$  powder via spray pyrolysis (ultrasonic and FEAG) has been previously reported [41]. Significant advance is shown due to the mixing of starting reactants at molecular scale, but obtaining of the pure garnet phase was hindered by retaining of amorphous phase or  $\text{Y}_4\text{Al}_2\text{O}_9$  (YAM) and  $\text{YAlO}_3$  (YAP) phases appearing. The lack of formation of YAG in all the spray pyrolysis experiments was ascribed to the short heating times and fast heating rates, which result-

ed in the formation of kinetic products. Therefore, annealing process at high temperatures was applied for the crystallization and activation of cerium-doped YAG particles.

Rationalization of the sequence for nanocrystalline YAG: $\text{Ce}^{3+}$  phase evolution in the particles synthesized by ultrasonic spray pyrolysis method through variation of processing parameters or precursors composition was also the topic of our research [17–22,34]. It was shown that particle morphological and structural characteristics are dependent on the applied synthesis methodology, especially regarding the precursors solution modification. Synthesis from common nitrates precursors was performed at 900°C in a tubular flow reactor using the air to carry the aerosol. Short residence time during synthesis resulted in multiphase powder generation. Beside garnet phase, YAM and  $\text{Y}_2\text{O}_3$  were also detected [18]. Synthesized particles were submicronic in size, highly spherical and un-ag-

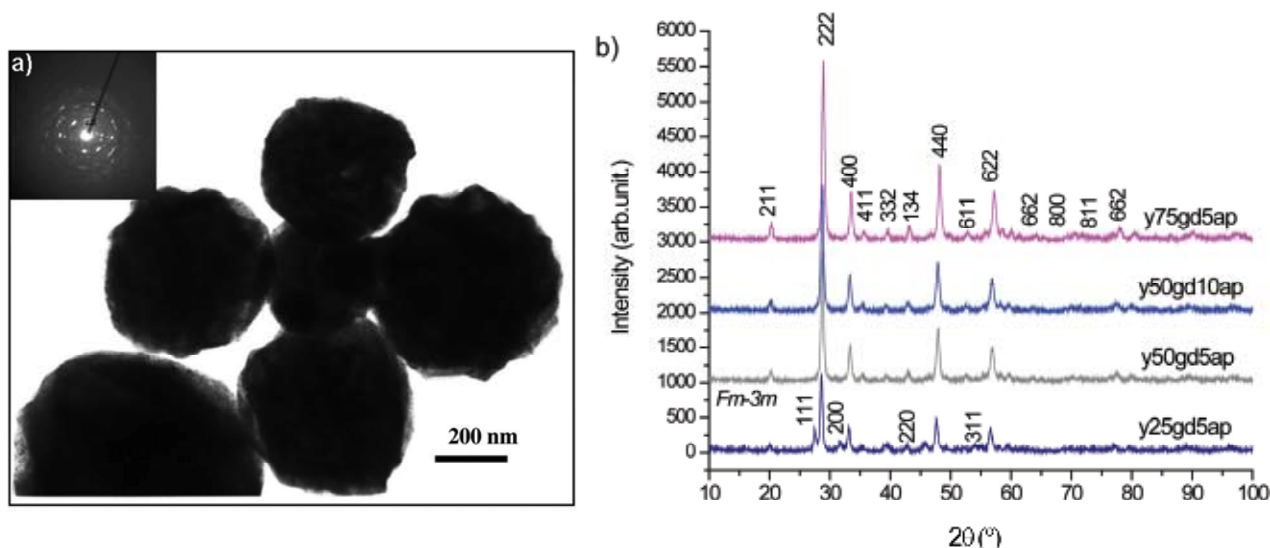


Figure 7. TEM/SAED image for as-prepared  $(\text{Y}_{0.50}\text{Gd}_{0.50})_2\text{O}_3:\text{Eu}^{3+}$  powder with 10 at% of  $\text{Eu}^{3+}$  (a) and XRD diffraction patterns of the as-prepared samples for  $(\text{Y}_{1-x}\text{Gd}_x)_2\text{O}_3:\text{Eu}^{3+}$  system (b)

Table 2. Main structural characteristics derived through Rietveld refinement and characteristics of the luminescent measurements for  $(\text{Y}_{1-x}\text{Gd}_x)_2\text{O}_3:\text{Eu}^{3+}$  system annealed at 1100°C [23]

	$(\text{Y}_{0.75}\text{Gd}_{0.25})_2\text{O}_3:\text{Eu}^{3+}$ 5 at% $\text{Eu}^{3+}$	$(\text{Y}_{0.5}\text{Gd}_{0.5})_2\text{O}_3:\text{Eu}^{3+}$ 5 at% $\text{Eu}^{3+}$	$(\text{Y}_{0.25}\text{Gd}_{0.75})_2\text{O}_3:\text{Eu}^{3+}$ 5 at% $\text{Eu}^{3+}$	$(\text{Y}_{0.5}\text{Gd}_{0.5})_2\text{O}_3:\text{Eu}^{3+}$ 10 at% $\text{Eu}^{3+}$
$cs$ [nm]	155.94	202.63	55.25	191.36
$a$ [Å]	10.667	10.724	10.771	10.730
$ms$ [%]	0.0329	0.0563	0.0333	0.0195
${}^5\text{D}_0 \rightarrow {}^7\text{F}_0$ ( $\text{C}_2$ ) [nm]	579.9	580.0	580.0	579.9
${}^5\text{D}_0 \rightarrow {}^7\text{F}_1$ ( $\text{S}_0$ ) [nm]	581.6	581.6	581.4	581.4
	586.8	586.9	587.1	586.9
${}^5\text{D}_0 \rightarrow {}^7\text{F}_1$ ( $\text{C}_2$ ) [nm]	592.3	592.3	592.2	592.2
	598.5	598.3	598.2	598.4
$\Delta E$ [ $\text{cm}^{-1}$ ]	333.2	324.7	316.1	327.5
$\tau({}^5\text{D}_0 \rightarrow {}^7\text{F}_2)$ [ms]	1.36	1.25	1.32	0.86
$\tau_{avr}({}^5\text{D}_1 \rightarrow {}^7\text{F}_2)$ [ $\mu\text{s}$ ]	14.3	13.9	13.6	/

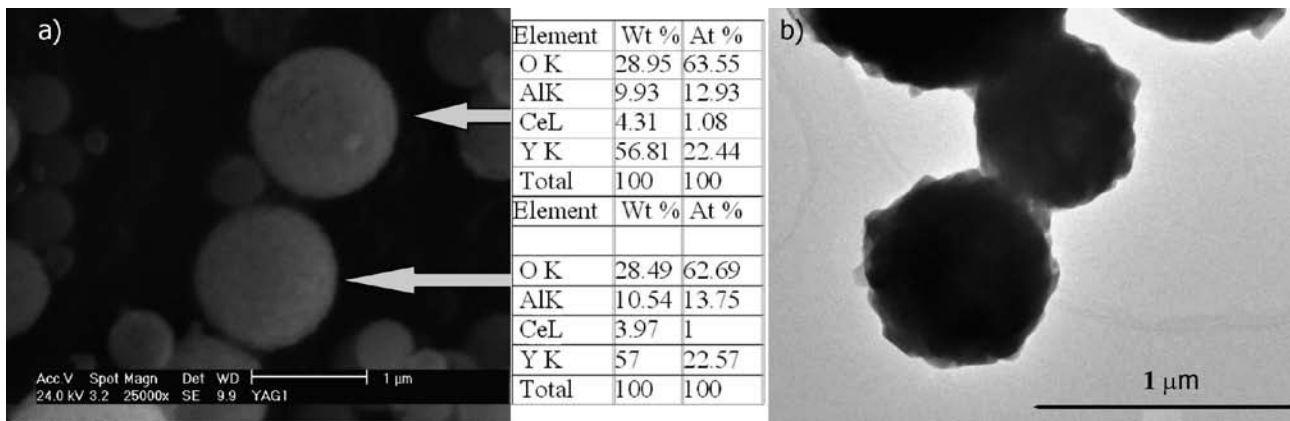


Figure 8. SEM/EDS of the YAG:Ce<sup>3+</sup> particles obtained through spray pyrolysis of nitrate solution at 900°C and annealed at 1000°C, 6 h (a); TEM of the YAG:Ce<sup>3+</sup> particles obtained through spray pyrolysis of nitrate solution at 320°C and annealed at 1000°C, 6 h (b)

glomerated. They exhibit rough surface implying that are built from primary nanoparticles [17]. Their general morphology did not changed significantly with annealing, but their roughness increase further due promoted crystallization affecting their specific surface [19]. Incorporation of Ce<sup>3+</sup> ions at the host is confirmed with the broad emission having peak maximum at 533 nm [17]. The interpretation of the thermo- and radio- luminescence signals from the YAG:Ce<sup>3+</sup> powders implies that the cerium ions are not readily accommodated on the YAG lattice sites during synthesis [12]. Even after annealing cerium ions do not offer a favourable excitation decay path; instead, there are broad emission bands typical of the host lattice defect sites and a very weak luminescence via the cerium on pathway near 300 nm. The complexity of the temperature dependence of the TL as a function of wavelength also suggests that a variety of independent defect sites contributes to the TL. They also indicated numerous anomalies in the temperature dependence of their luminescence lifetime data.

To investigate the nature of the multiphase powder obtaining, an amorphous material with composition corresponding to yttrium aluminum garnet phase

with same content of cerium has been synthesized at 320°C using a similar spray pyrolysis route. Precursor-derived amorphous phase crystallized at temperatures as high as 900 and 1000°C gave multiphase powders with different compositions after 3 h of annealing (YAP, YAP, YAM), while prolongation of treatment at higher temperature result in pure YAG phase formation (Fig. 8) [20].

In order to achieve additional heating during YAG:Ce<sup>3+</sup> synthesis urea-assisted spray pyrolysis was employed [25]. This route can be regarded as a self-combustion synthesis confined within a droplet where urea acts as an *in-situ* source of thermal energy due to its decomposition. The as-prepared non-agglomerated amorphous powder has broad particle size distribution (200–1400 nm) (Fig. 9). They were additionally thermally treated in air at 1000 and 1100°C for 6h preserving their morphological characteristics. Despite of precursor modification during synthesis, performed annealing did not yielded pure YAG:Ce<sup>3+</sup> product. While lower temperature is favourable for YAP and YAM phase segregation, increase of heating temperature enhanced YAG phase formation with YAM phase retention.

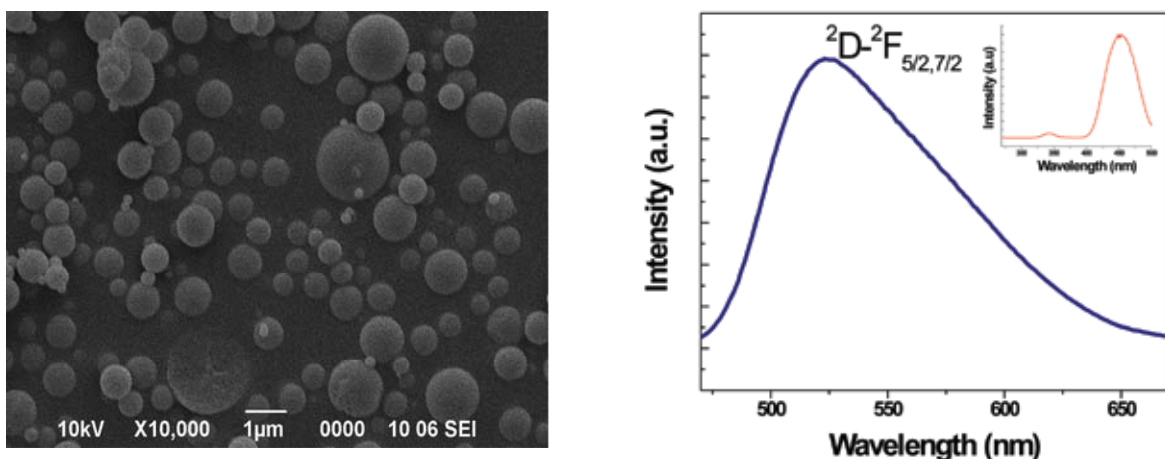
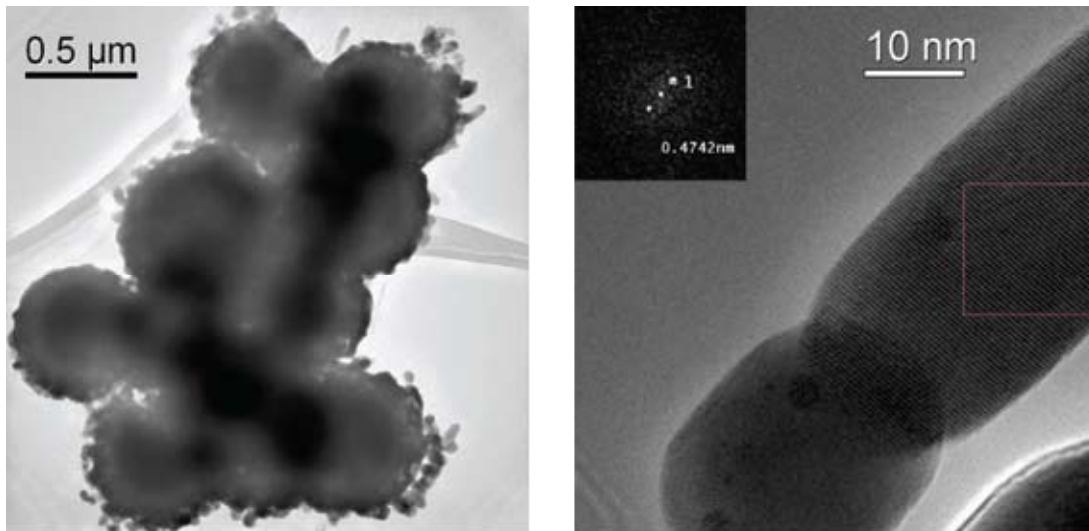


Figure 9. SEM of the as-prepared YAG:Ce<sup>3+</sup> particles obtained through urea-assisted spray pyrolysis at 900°C; PL spectra of particles treated at 1100°C (3 h)



**Figure 10.** TEM/HRTEM/FFT of the YAG:Ce<sup>3+</sup> particles obtained from polymeric precursor solution through spray pyrolysis at 900°C; annealed at 1100°C; FFT inset confirm *Ia-3d* phase formation (211) plane

Having this in mind, preservation of the molecular homogeneity during precursor synthesis was done through polymerization with an organic complexing agent EDTA and ethylene glycol (EG) [22]. Two reactions are involved, a complex formation between EDTA and metals (via four carboxylate and two amine groups) and esterification between EDTA and EG. Ultrasonically generated aerosol droplets were decomposed at 600°C in argon atmosphere. Following the initial attempt in providing pure YAG:Ce<sup>3+</sup> phase generation the particles were additionally thermally treated for 3 h in air at 1000°C and 1100°C. Comprehensive structural analysis implied that garnet phase was formed without contamination of other phase having different aluminum yttrium composition even at the lower annealing temperature and in a much shorter time. The spherical dense particles comprised grained-like structure, since they are composed of nanosized garnet monocrystals (Fig. 10). Although uncompleted, cerium incorporation in garnet matrix is confirmed by broad green-yellow emission spectra in the range of 470–670 nm peaking at 521 nm. With this optimization of the spray pyrolysis reaction conditions towards synthesis of pure, unagglomerated YAG:Ce<sup>3+</sup> particles with spherical shape and filled morphology were achieved.

#### IV. Conclusions

Aerosol route represents a versatile synthesis method for processing novel functional materials. An insight into the diversity of this method and materials that could be produced was briefly reviewed. Particularly, it was shown that spray pyrolysis is one of the simplest among them and is capable in ensuring particle spherical morphology, good crystallinity and uniformity in size and shape. Those characteristics are found to be of great value since they result in well defined phosphor powder characteristics essential for achieving higher brightness and resolution in

displays. Superior structural, morphological and functional properties of Gd<sub>2</sub>O<sub>3</sub>:Eu, Y<sub>2</sub>O<sub>3</sub>:Eu, (Y<sub>1-x</sub>Gd<sub>x</sub>):Eu and Y<sub>3</sub>Al<sub>5</sub>O<sub>12</sub>:Ce powders are presented and correlated with the processing parameters applied facilitating further tailoring of specific properties in these materials.

**Acknowledgement** This research is financially supported through the Project No. 142010 of the Ministry of Science and Technology of the Republic of Serbia and COST 539 Action.

#### References

1. H. Tuller, "Solid state electrochemical systems-opportunities for nanofabricated or nanostructured materials", *J. Electroceram.*, **1** [3] (1997) 211–218.
2. G.L. Messing, S.-C. Zhang, G.V. Jayanthi, "Ceramic powder synthesis by spray pyrolysis", *J. Am. Ceram. Soc.*, **76** [11] (1993) 2707–2726.
3. L. Madler, "Liquid-fed aerosol reactors for one-step synthesis of nano-structured particles", *KONA*, **22** (2004) 107–119.
4. R.J. Lang, "Ultrasonic atomization of liquids", *J. Acoust. Soc. Am.*, **34** (1962) 6–8.
5. O. Milosevic, L. Mancic, M.E. Rabanal, L.S. Gomes, K. Marinkovic, "Aerosol route in processing of nanostructured functional materials", *KONA*, **27** (2009) 84–106.
6. R. Maric, T. Fukui, S. Ohara, H. Yoshida, M. Nishimura, T. Inagaki, K. Miura, "Powder prepared by spray pyrolysis as an electrode material for solid oxide fuel cells", *J. Mater. Sci.*, **35** (2000) 1–8.
7. Z.V. Marinkovic, L. Mancic, R. Maric, O. Milosevic, "Preparation of nanostructured Zn-Cr-O spinel powders by ultrasonic spray pyrolysis", *J. Eur. Ceram. Soc.*, **21** (2001) 2051–2055.
8. K. Okuyama, I.W. Lenggoro, "Preparation of nanoparticles via spray route", *Chem. Eng. Sci.*, **58** (2003) 537–547.

9. Z.V. Marinkovic, L. Mancic, O. Milosevic, "Nature of structural changes in nanocrystalline ZnO powders under linear heating conditions", *J. Eur. Ceram. Soc.*, **24** (2004) 1929–1933.
10. V.M. Djinovic, L.T. Mancic, G.A. Bogdanovic, P.J. Vulic, G. del Rosario, T.J. Sabo, O.B. Milosevic, "Aerosol synthesis of pure and Pt-doped ZnO particles using nitrate and pdda-Pt(IV) complex solutions", *J. Mater. Res.*, **20** [1] (2005) 102–113.
11. S. Grguric-Sipka, T. Sabo, L. Mancic, O. Milosevic, "Aerosol synthesis of ruthenium doped ZnO fine particles", *J. Aerosol Sci.*, **35** (2004) S183–184.
12. Y. Wang, O. Milosevic, L. Gómez, M.E. Rabanal, J.M. Torralba, B. Yang, P.D. Townsend, "Thermoluminescence responses from europium doped gadolinium oxide", *J. Phys. Cond. Matter*, **18** (2006) 9257–9272.
13. M.E. Rabanal, L.S. Gómez, A. Khalifa, J.M. Torralba, L. Mancic, O. Milosevic, "Structural properties of europia-doped-gadolinia synthesized through aerosol", *J. Eur. Ceram. Soc.*, **27** [13-15] (2007) 4325–4328.
14. L.S. Gómez, M.E. Rabanal, J.M. Torralba, L. Mancic, O. Milosevic, "Structural and morphological study of nanoceramics prepared by spray pyrolysis", in *Characterization & Control of interfaces for High Quality Advanced materials - Ceram.Trans.*, **198** (2007) 193–197.
15. K. Marinkovic, L. Mancic, L. Gomez, M.E. Rabanal, M. Dramicanin, O. Milosevic, "Nanostructured ( $Y_{1-x}Gd_x$ )<sub>2</sub>O<sub>3</sub>:Eu<sup>3+</sup> powders obtained through aerosol synthesis", *ICCCI 2009*, Kurashiki, Japan, 2009.
16. K. Marinkovic, L. Mancic, L. Gomez, M.E. Rabanal, M. Dramicanin, O. Milosevic, "Photoluminescent properties of nanostructured Y<sub>2</sub>O<sub>3</sub>:Eu<sup>3+</sup> powders obtained by aerosol synthesis", *ICOM 2009*, Herceg Novi, Montenegro, 2009.
17. G. del Rosario, S. Ohara, L. Mancic, O. Milosevic, "Characterization of YAG:Ce powders thermal treated at different temperatures", *Appl. Surf. Sci.*, **238** [1-4] (2004) 469–474.
18. O. Milosevic, L. Mancic, S. Ohara, G. Rosario, P. Vulic, "Aerosol synthesis and phase development in Ce-doped nanophased yttrium-aluminum garnet (Y<sub>3</sub>Al<sub>5</sub>O<sub>12</sub>:Ce) particles", in *Characterisation and Control of Interfaces for High Quality Advanced Materials- Ceram.Trans.*, **146** (2004) 435–441.
19. L. Mancic, G. del Rosario, Z. Marinkovic, O. Milosevic, "Detailed structural characterization of phosphor YAG:Ce particles obtained via spray pyrolysis", *Mater. Sci. Forum*, **518** (2006) 107–112.
20. L. Mancic, G. del Rosario, Z.V. Marinkovic-Stanojevic, O. Milosevic, "Phase evolution in Ce doped yttrium aluminum based particles derived from aerosol", *J. Eur. Ceram. Soc.*, **27** (2007) 4329–4332.
21. Lj. Kandic, K. Marinkovic, L. Mancic, G. del Rosario, O. Milosevic, "Low temperature aerosol synthesis of YAG:Ce<sup>3+</sup> nanostructures: Comparative study of the XRPD microstructural parameters", *Mater. Sci. Forum*, **555** (2007) 395–400.
22. L. Mancic, K. Marinkovic, B. Marinkovic, M. Dramicanin, O. Milosevic, "YAG:Ce<sup>3+</sup> nanostructured particles obtained via spray pyrolysis of polymeric precursor solution", *J. Eur. Ceram. Soc.*, **30** (2010) 577–582.
23. K. Marinkovic, "Structural, morphological and functional properties of nanostructured rare-earth oxides obtained through aerosol synthesis", *Master Science Thesis*, Belgrade University, 2009.
24. L.S. Gomez, "Sintesis y caracterization de oxidos nanoestructurados de gadolinio e ytrio dopados con europio obtenidos mediante el metodo de spray pirolisis", *Ph.D. Thesis*, University Carlos III, Madrid, 2009.
25. K. Marinkovic, L. Mancic, V.B. Pavlovic, M. Dramicanin, O. Milosevic, "Urea-assisted self-combustion aerosol synthesis of Y<sub>3</sub>Al<sub>5</sub>O<sub>12</sub>:Ce<sup>3+</sup>", *YUCOMAT*, Herceg Novi, Montenegro, 2008.
26. P.D. Rack, P.H. Holloway, "The structure, device physics and material properties of thin film electroluminescent displays", *Mater. Sci. Eng.*, **4** (1998) 171–219.
27. R.C. Ropp, *Luminescence and the Solid State*, Elsevier Science Publishers B.V., New York, 1991.
28. M. Maghrabi, P.D. Townsend, G. Vazquez, "Low temperature luminescence from the near surface region of Nd:YAG", *J. Phys.: Condens. Matter*, **13** (2001) 2497–2515.
29. E. Zych, C. Brecher, A.J. Wojtowicz, H. Lingertat, "Luminescence properties of Ce-activated YAG optical ceramic scintillator materials", *J. Lumin.*, **75** (1997) 193–203.
30. H. Koo, S. Ju, D.S. Jung, S.K. Hong, D.Y. Kim, Y.C. Kang, "Morphology control of Gd<sub>2</sub>O<sub>3</sub>:Eu phosphor particles with cubic and monoclinic phases prepared by high temperature spray pyrolysis", *Jap. J. Appl. Phys.*, **45**, [6A] (2006) 5018–5022.
31. J.S. Bae, S.S. Yi, J.H. Kim, K.S. Shim, B.K. Moon, J.H. Jeong, Y.S. Kim, "Crystalline-phase-dependent red emission behaviours of Gd<sub>2</sub>O<sub>3</sub>:Eu<sup>3+</sup> thin-film phosphors", *Appl. Phys. A*, **82**, [2] (2006) S.369–372.
32. D.J. Seo, Y.C. Kang, S.B. Park, "The synthesis of (Y<sub>1-x</sub>Gd<sub>x</sub>)<sub>2</sub>O<sub>3</sub>:Eu phosphor particles by flame spray pyrolysis with LiCl flux", *Appl. Phys. A*, **77** (2003) 659–663.
33. O. Milosevic, R. Maric, S. Ohara, T. Fukui, "Structural and luminescence properties of Gd<sub>2</sub>O<sub>3</sub>:Eu<sup>3+</sup> and Y<sub>3</sub>Al<sub>5</sub>O<sub>12</sub>:Ce<sup>3+</sup> phosphor particles synthesized via aerosol", *Ceram. Trans.*, **112** (2001) 101–106.
34. O. Milosevic, L. Mancic, M.E. Rabanal, B. Yang, P.D. Townsend, "Structural and luminescence properties of Gd<sub>2</sub>O<sub>3</sub>:Eu<sup>3+</sup> and Y<sub>3</sub>Al<sub>5</sub>O<sub>12</sub>:Ce<sup>3+</sup> phosphor particles synthesized via aerosol", *J. Electrochem. Soc.*, **152** (2005) G707–713.
35. S. Jung, Y.C. Kang, J.H. Kim, "Generation of phosphor particles for photoluminescence applications by spray pyrolysis", *J. Mater. Sci.*, **42** (2007) 9783–9794.

36. O. Malta, E. Antic-Fidancev, M. Lemaitre-Blaise, A. Milicic-Tang, M. Taibi, “The crystal field strength parameter and the maximum splitting of the  ${}^7F_1$  manifold of the  $\text{Eu}^{3+}$  ion in oxides”, *J. Alloys Compd.*, **228** (1995) 41–44.
37. O. Pons, Y. Moll, A. Huignard, E. Antic-Fidancev, P. Aschehoug, B. Viana, E. Millon, J. Perrière, C. Garapon, J. Mugnier, “ $\text{Eu}^{3+}$ - and  $\text{Tm}^{3+}$ -doped yttrium oxide thin films for optical applications” *J. Lumin.*, **87-89** (2000) 1115–1117.
38. D.R. Tallant, C.H. Seager, R.L. Simpson, “Energy transfer and relaxation in europium-activated  $\text{Y}_2\text{O}_3$  after excitation by ultraviolet photons”, *J Appl. Phys.*, **91** (2002) 4053–4064.
39. Ž. Andrić, M.D. Dramićanin, M. Mitrić, V. Jokanović, A. Bessiere, B. Viana, “Polymer complex solution synthesis of  $(\text{Y}_x\text{Gd}_{1-x})_2\text{O}_3:\text{Eu}^{3+}$  nanopowder”, *Opt. Mater.*, **30** (2008) 1023–1027.
40. H. Yang, D-K. Lee, Y-S. Kim, “Spectral variations of nano-sized  $\text{Y}_3\text{Al}_5\text{O}_{12}:\text{Ce}$  phosphors via codoping/substitution and their white LED characteristics”, *Mater. Chem. Phys.*, **114** (2009) 665–669.
41. Y.C. Kang, I.W. Lenggoro, S.B. Park, K. Okuyama, “YAG:Ce phosphor particles prepared by ultrasonic spray pyrolysis”, *Mater. Res. Bull.*, **35** (2000) 789–798.

